Bulletin of the Mineral Research and Exploration

http://bulletin.mta.gov.tr

Edge enhancement of potential field data using the enhanced gradient (EG) filter

Hazel Deniz TOKTAY[a*], Korimilli Naga Durga PRASAD[b] and Ahmad ALVANDI[c]

[a] *İstanbul University-Cerrahpaşa, Faculty of Engineering, Department of Geophysical Engineering, Büyükçekmece Campus, İstanbul, Türkiye*

[b] *Council of Scientific and Industrial Research -National Geophysical Research Institute, Gravity and Magnetic Studies Group, Uppal Road, Hyderabad, 500007, Telangana, India*

[c] *University of Tehran, Institute of Geophysics, Tehran, Iran*

Research Article

Keywords:
Edge Detection, Gradient, Potential Field, Mapping.

ABSTRACT

Potential field data play a critical role in interpreting various geologic structural features through edge detection filters that aid in mapping subsurface structural features. For this purpose, various filters have been introduced in recent years to determine lateral boundaries. However, each of these filters has its limitations and advantages. This study presents a new edge enhancement filter named Enhanced Gradient (EG) based on the Richards function and applies it to potential field data for structural mapping. The EG is tested on two dimensional (2D) and three dimensional (3D) synthetic magnetic models with sources buried at different depths and variable properties. The results from the EG filter provide more accurate and higher resolution horizontal boundaries and can avoid creating the false edges in the output results. In addition, the proposed filter was examined using aeromagnetic data from the Indiana region in the USA. The primary and secondary faults and geological formations are recognizable in the EG image. The results of the EG map will allow us to improve the qualitative interpretation of potential field anomalies in studying the structural and tectonic geology of the Indiana region in the USA.

Received Date: 01.05.2023
Accepted Date: 14.06.2023

1. Introduction

Gravity and magnetics are widely used geophysical methods for understanding subsurface structures and tectonics. Some of the applications of the method include mineral resource exploration, hydrocarbon exploration, crustal deformation studies, and surface and subsurface structural mapping. Much emphasis can be made on the structural feature delineation that helps us understand various geological structural boundaries buried at depth. Determining the horizontal boundaries of these buried sources and delineating the lateral extents is of prime importance. There are many filters used to determine the edge of potential field anomalies. Each filter has advantages and limitations (Alvandi et al., 2022; Prasad et al., 2022*a*; Ibraheem et al., 2023). A standard method for identifying horizontal boundaries called the total horizontal derivative (THDR), was introduced by Cordell and Grauch (1985). The THDR procedure is less sensitive to noise in the data and is suitable for determining shallow sources (Phillips, 2002; Pham et al., 2021; Alvandi and Ardestani, 2023). The maximum amplitudes of the THDR are located over the boundaries of the geological contact, and it is defined in Equation 1 as follows:

Citation Info: Toktay H. D., Prasad K. N. D., Alvandi A. 2024. Edge enhancement of potential field data using the enhanced gradient (EG) filter. Bulletin of the Mineral Research and Exploration 174, 55-66. https://doi.org/10.19111/bulletinofmre.1386653

**Corresponding author: Hazel Deniz TOKTAY, hazel.deniztoktay@iuc.edu.tr*

$$THDR = \sqrt{\left(\frac{\partial T}{\partial x}\right)^2 + \left(\frac{\partial T}{\partial y}\right)^2} \quad (1)$$

where T is the magnetic or gravity field, $\frac{\partial T}{\partial x}$ and $\frac{\partial T}{\partial y}$ are its first-order derivatives in the x and y directions, respectively (Blakely and Simpson, 1986; Prasad et al., 2022*b*).

The 3D analytical signal amplitude (ASA) is a popular procedure for identifying the lateral boundaries of potential field anomalies, given by Equation 2 (Nabighian, 1984; Roest et al., 1992).

$$ASA = \sqrt{\left(\frac{\partial T}{\partial x}\right)^2 + \left(\frac{\partial T}{\partial y}\right)^2 + \left(\frac{\partial T}{\partial z}\right)^2} \quad (2)$$

where $\frac{\partial T}{\partial z}$ is a first-order vertical derivative of the potential field. On the other hand, maximum ASA values are very sensitive to depth and are only located over the horizontal boundaries when the source's depth is shallow. However, THDR and ASA are ineffective in balancing sources simultaneously at different depths (Pham et al., 2021, 2022; Prasad et al., 2022*a*, 2022*b*; Alvandi et al., 2023).

In order to determine the horizontal boundaries of the shallow and deep anomalies simultaneously, a wide range of phase-based filters has been introduced. The tilt derivative (TDR) filter was introduced as the first to determine the edge of potential field anomalies. (Miller and Singh, 1994). The TDR uses the amplitude of the THDR to normalize the vertical derivative. Although the vertical derivative and THDR are both weak for deeper sources edge detection, the TDR (Equation 3) using the ratio of the vertical derivative to the THDR has overcome this problem and equalized the deep and shallow sources. The amplitude of TDR over the source is positive, with zero amplitude over the edge (Zero vertical derivative and maximum horizontal gradient), and elsewhere, it is negative.

$$\mathrm{TDR} = \mathrm{atan}\left(\frac{\frac{\partial \mathrm{T}}{\partial \mathrm{z}}}{\mathrm{THDR}}\right) \quad (3)$$

The TDR amplitude variations have a specific range, ±90° (Miller and Singh, 1994). This filter is insensitive to source depth compared to THDR and ASA filters and does not completely balance the source edges buried at various depths. However, with increasing depth, TDR loses its sharpness so that the edges of the anomaly become blurred (Pham et al., 2018).

Wijns et al. (2005) developed another phase-based filter called theta map (TM) filter. The TM uses the ASA to normalize the THDR. The amplitude of the filter is minimal over the source edges. The TM filter is sensitive to depth sources and does not detect deep and thin source edges well (Prasad et al., 2022*a*). The TM amplitude variations have a specific range, between 0°-90° (Equation 4).

$$\mathrm{TM} = \mathrm{acos}\left(\frac{\mathrm{THDR}}{|\mathrm{ASA}|}\right) \quad (4)$$

Cooper and Cowan (2006) have developed modified versions of the total horizontal gradient and vertical derivative to improve the resolution of edges. The horizontal tilt derivative (TDX) filter is a normalized form of THDR amplitude to the absolute value of $\frac{\partial \mathrm{T}}{\partial \mathrm{z}}$ and is represented in Equation 5.

$$\mathrm{TDX} = \mathrm{atan}\left(\frac{\mathrm{THDR}}{\left|\frac{\partial \mathrm{T}}{\partial \mathrm{z}}\right|}\right) \quad (5)$$

The TDX filter is the inverse of the tilt derivative filter, as it performs equally well with both shallow and deep anomalies. In addition, these filters do not indicate the edges of interfering sources (Zuo et al., 2018; Prasad et al., 2022*b*).

Castro et al. (2018) introduced another balanced-edge detection method, the combined tilt derivative filters (TDR±TDX) and is defined in Equation 6 as:

$$\begin{cases} \mathrm{TDX} + \mathrm{TDR} = \frac{\pi}{2} & \text{if } \mathrm{TDR} > 0 \\ \mathrm{TDR} - \mathrm{TDX} = \frac{-\pi}{2} & \text{if } \mathrm{TDR} < 0 \end{cases} \quad (6)$$

The TDR-TDX filter produces sharp peaks over the source centers, while the TDR + TDX filter creates a plateau. In TDR±TRX for deep-seated sources, the limits of body edges will appear wider than the actual edges (Castro et al., 2018).

2. Proposed Method

This paper proposes a novel edge detection filter called Enhanced Gradient (EG) based on the Richards function for balancing the edges of magnetic and gravity sources. The EG (Equation 7) filter has a near-

identical shape to the arc-tan function (Richards, 1959), often used for potential field data edge detection.

$$EG = \left(1 + \exp\left(\frac{-\frac{\partial BT}{\partial Z}}{\sqrt{\left(\frac{\partial BT}{\partial x}\right)^2 + \left(\frac{\partial BT}{\partial y}\right)^2}}\right)\right)^{-\alpha} \quad (7)$$

where

$$BT = \frac{(THDR)^{\alpha}}{1+\sqrt{(H_X(THDR))^2 + (H_Y(THDR))^2 + THDR^2}} \quad (8)$$

where H_X and H_Y are the Hilbert transform of the total horizontal gradient amplitude filter (Cooper, 2009) and $\propto$ a positive number.

3. Evaluation of Alpha ($\propto$)

A synthetic gravity model consisting of three prisms, with different physical properties buried at different depths and density contrasts, is created. The physical and geometrical properties of the bodies are represented in Figure 1a. for evaluating the alpha

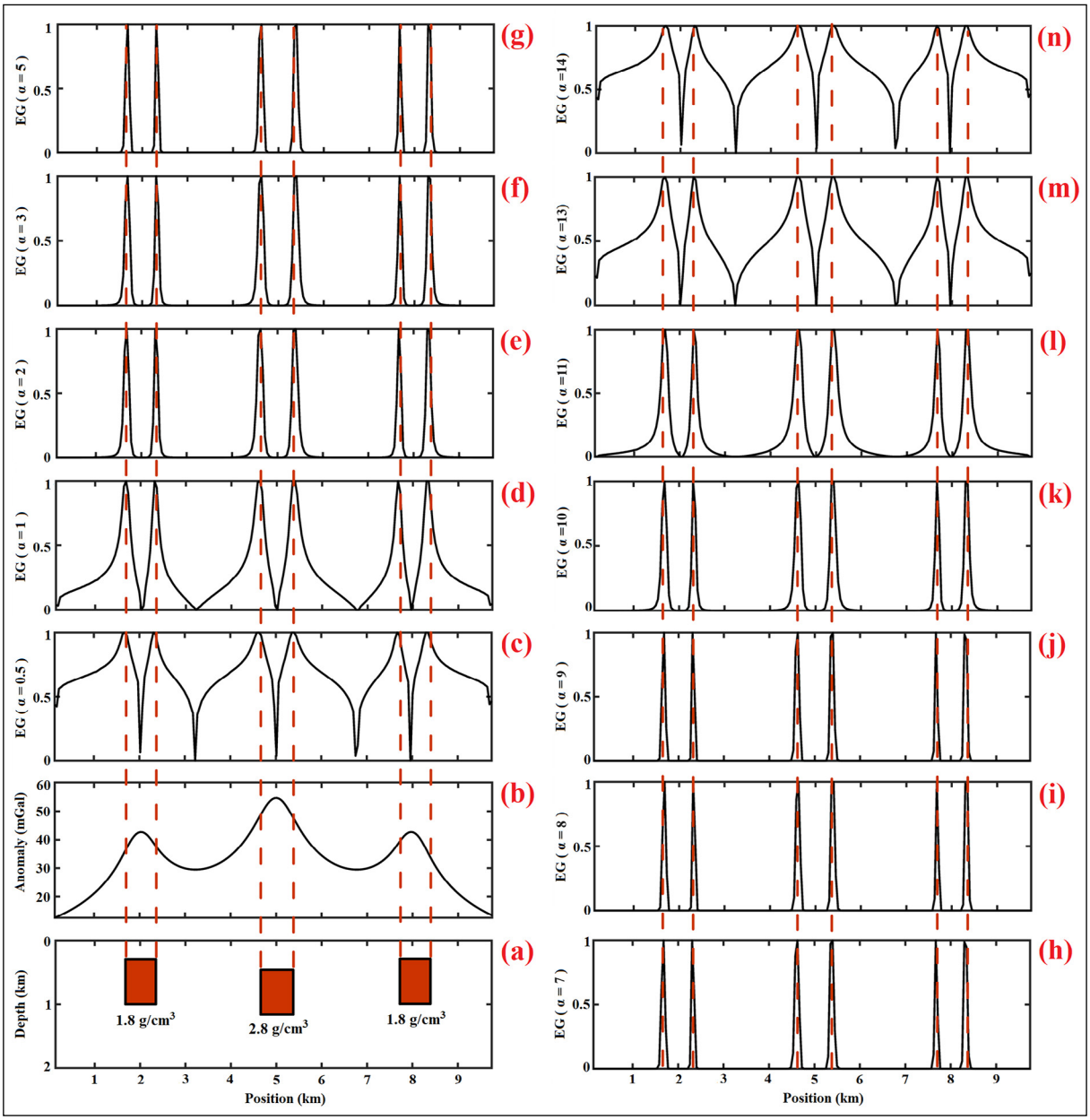

Figure 1- Evaluation of alpha (α) parameter in the EG over synthetic gravity anomaly; a) Schematic representation of synthetic model, b) the gravity anomaly response over the prismatic bodies. The response of the EG at c) α=0.5, d) α=1, e) α=2, f) α=3, g) α=5, h) α=7, i) α=8, j) α=9, k) α=10, l) α=11, m) α=13, n) α=14.

(∝) value to the proposed EG function. The schematic model is shown in Figure 1a, with the computed anomaly response presented in Figure 1b. The EG is applied to the computed gravity anomaly with values increasing from 0.5 to 14 (Figure 1c to Figure 1n). The results show that the amplitude response of the proposed filter is maximum over the edges. The filter produces sharp edges when the ∝ value is two and maintains its sharpness till ∝ the value is 10. The detected edges lose the sharp character and become vague when the ∝ value is more than 10. Therefore, to extract the effectiveness of the filter, a ∝ value of 2-10 can be used for the best results. In the present study, a ∝ value of 2 is fixed to all the synthetic and real data models.

4. Application Over the 2D Synthetic Magnetic Model

A synthetic magnetic model consisting of three prisms with different physical properties buried at different depths is developed. The physical and geometrical properties of the bodies are represented in Figure 2a. The magnetic response of the synthetic model is presented in Figure 2b, and its reduced-to-pole (RTP) magnetic anomaly is presented in

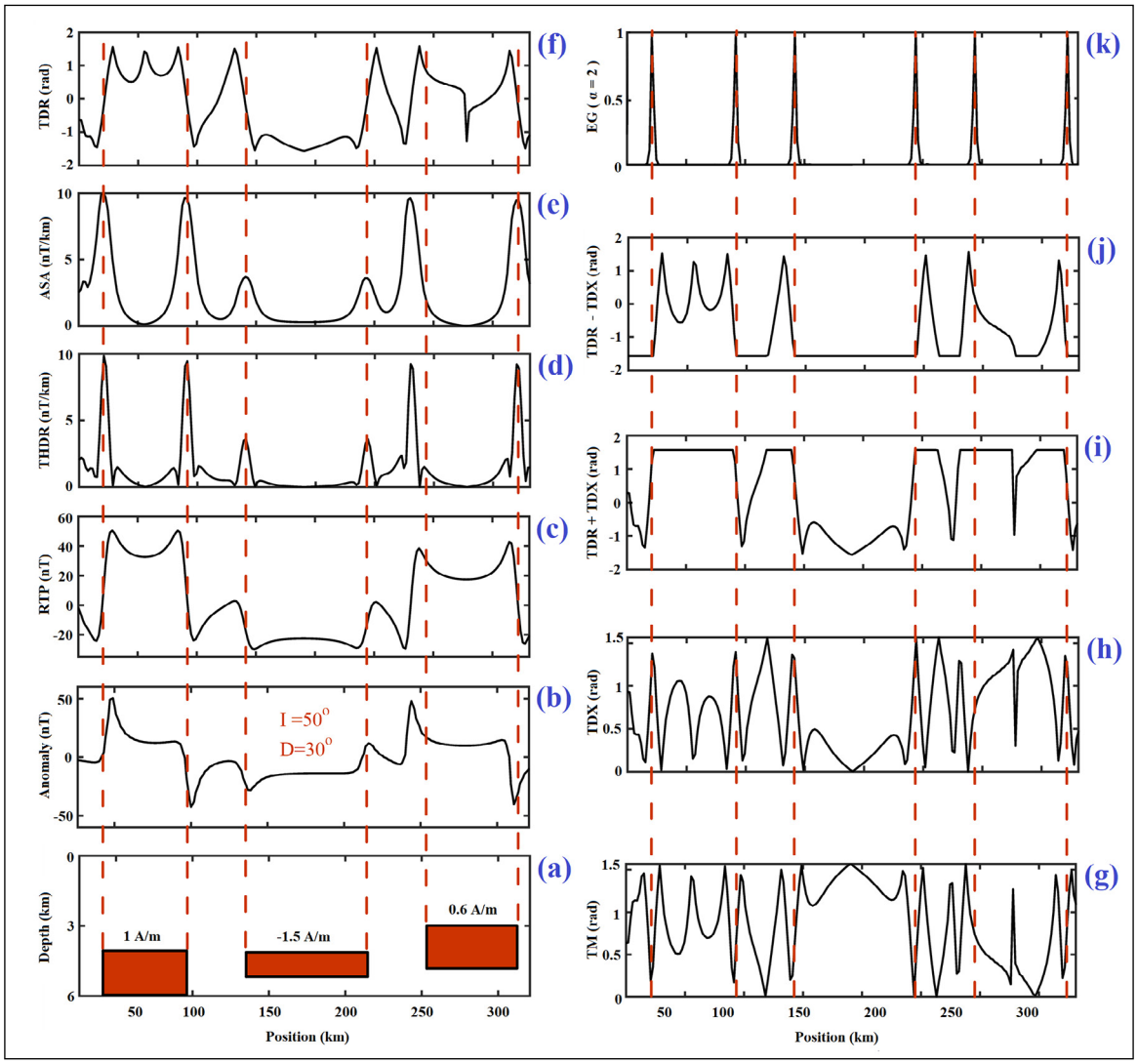

Figure 2 - The response of various edge detection techniques over a synthetic magnetic model; a) Schematic representation of synthetic model, b) the magnetic anomaly response over the three prismatic bodies, c) the reduced-to-pole magnetic anomaly response over the three prismatic bodies. The response of various filters are presented as d) THDR, e) ASA, f) TDR, g) TM, h) TDX, i) TDR + TDX, j) TDR – TDX and k) enhanced gradient filter.

Figure 2c. The response of the various conventional edge detection filters is represented in Figures 2d to 2j. It is obvious from the response that when the magnetic data is subjected to different conventional filters (Figure 2d to 2j), the response is better analyzed in THDR (Figure 2d), ASA (Figure 2e). However, the response is not balanced for the shallow and deeper bodies. The rest of the filters have spurious and false edges, making the interpretation more complex. When the Enhanced Gradient filter with $\propto = 2$ is applied to the RTP magnetic anomaly, the amplitude response maxima show a clear demarcation of the edges of the prismatic bodies (Figure 2k). The maxima of the response are over the edge of the body. Moreover, we can observe a balanced image from the sources buried at shallower and deeper depths.

5. Application Over the 3D Synthetic Magnetic Model

To illustrate the robustness of the proposed filter, a synthetic magnetic model with ten prismatic bodies is constructed. The schematic model of the synthetic magnetic model is shown in Figure 3a, with the nomenclature of the prismatic bodies in Figure 3b. The total magnetic intensity (TMI) is calculated on a 200×200 km^2 grid with a grid spacing of 1 km along the east-west and north-south directions (Figure 4a). The magnetic inclination and declination of all prisms are 90° and 0°, respectively. The magnetic anomaly is reduced to pole. The dimension and properties of the prismatic bodies are shown in Table 1.

The response of the THDR and ASA filters are shown in Figures 4b and 4c, respectively. Shallow

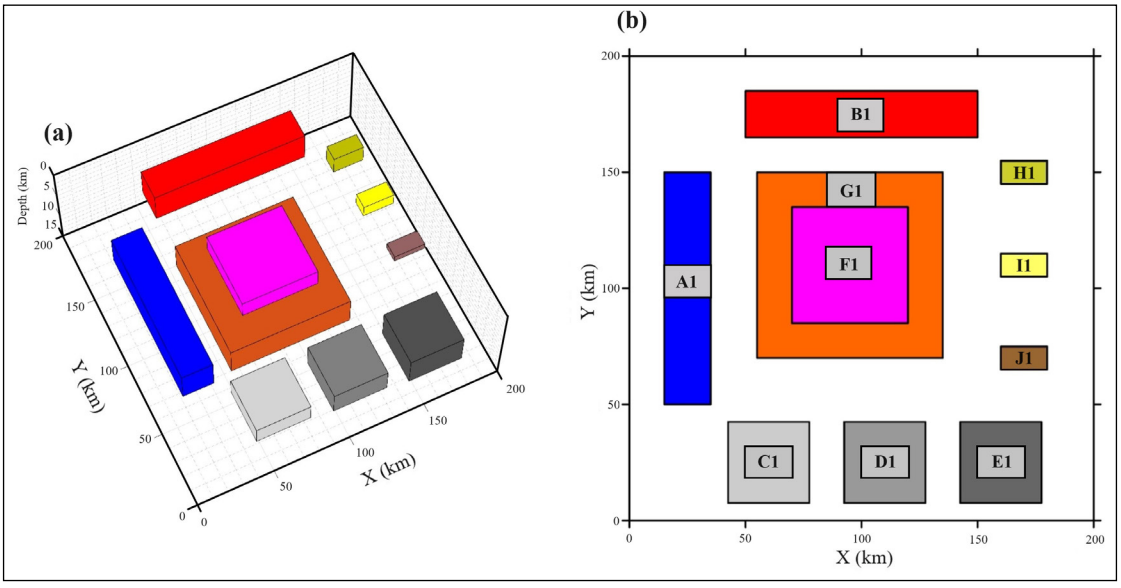

Figure 3- Schematic representation of the synthetic model (magnetic) in a) three-dimensional view and b) planar view with nomenclature of different prismatic bodies.

Table 1- The parameters of the prismatic bodies used to generate magnetic anomaly over the 3D synthetic model. All the dimensions are in kilometers.

Property	A1	B1	C1	D1	E1	F1	G1	H1	I1	J1
Xc	25	100	60	110	160	95	95	170	170	170
Yc	100	175	25	25	25	110	110	150	110	70
Width	20	100	35	35	35	50	80	20	20	20
Height	100	20	35	35	35	50	80	10	10	10
Top Depth	2	2	5	5	5	5	10	3	2	1
Thickness	5	5	3	4	5	3	5	3	2	1

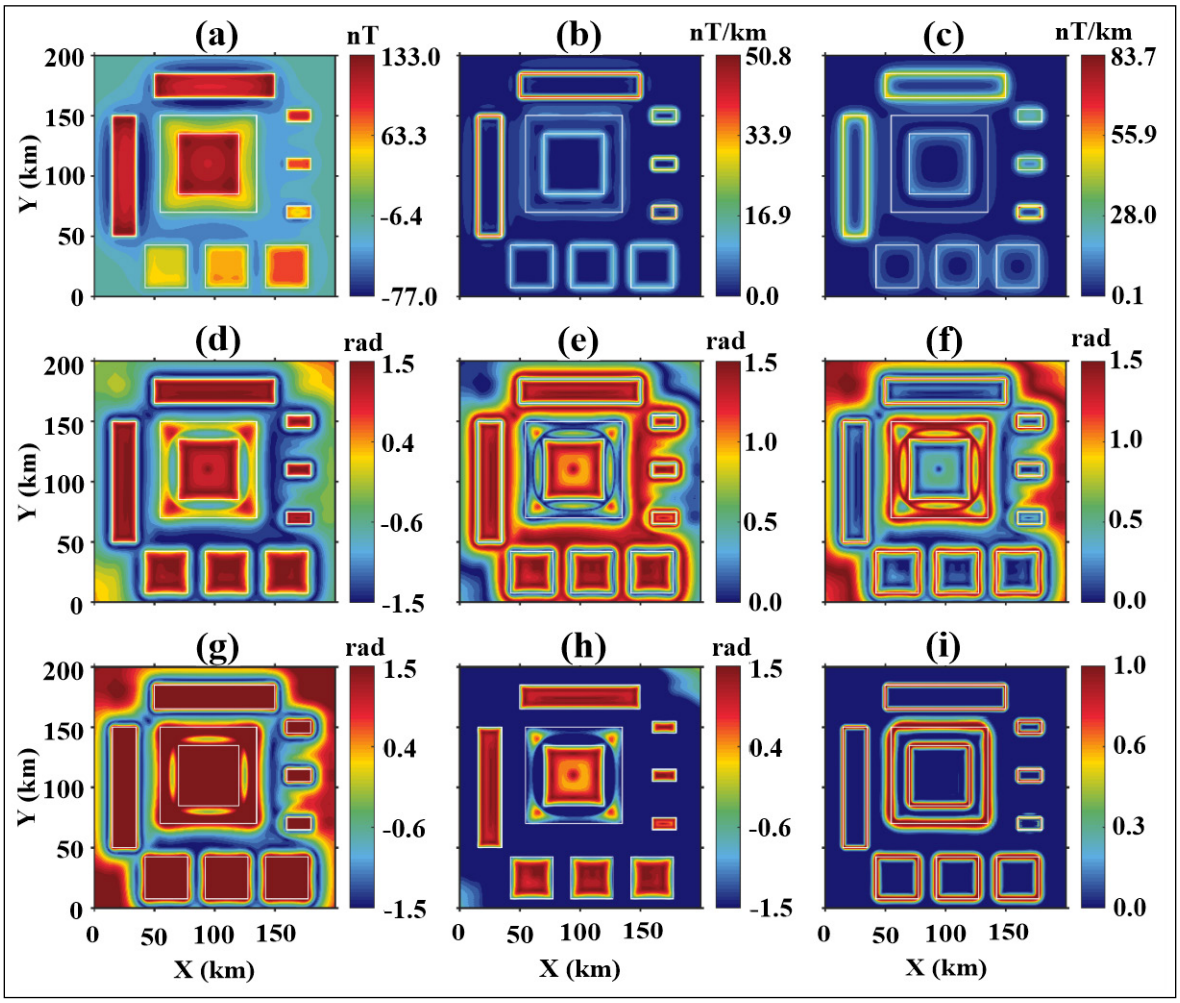

Figure 4- The magnetic anomaly is shown in a); All the 10 bodies are positively magnetized. The response of various edge detection filters are b) THDR, c) ASA, d) TDR, e) TM, f) TDX, g) TDR + TDX, h) TDR – TDX and i) Enhanced gradient filter (The white line represents the real prism edge).

seated bodies dominate the response. The edges detected from the deep-seated bodies are blurred. The filters TDR (Figure 4d), TM (Figure 4e), TXD (Figure 4f), TDR+TDX (Figure 4g), and TDR-TDX (Figure 4h) are found to produce spurious and false boundaries. The response of the EG filter at an alpha value of 2 is presented in Figure 4i shows that the proposed filter successfully delineates the edges of all the prismatic bodies buried at different depths. The filter produced a balanced image of the edges. The stability of the filter is also tested by applying negative magnetization to three bodies (blocks of 2, 4, and 9, as shown in Figure 5) which proved that the EG response was similar to the case discussed above. 4% Gaussian noise to the magnetic anomaly with a standard deviation of 0.5 nT and the results are shown in Figure 6, which shows a noisy response from all the filters where the EG filter proves to be better.

Any edge detection filter applied to the noisy data may not give a clear image of the subsurface structures (Pham et al., 2021; Prasad et al., 2022*a*), so we continued the anomaly to 500 m upward (Figure 7a). Figure 7b-j shows the results of the THDR, ASA, TDR, TM, TDX, TDR+TDX, TDR-TDX and EG after upward continuation of the data. THDR (Figure 7b) and ASA (Figure 7c) produced edges and the noise's influence is not much compared to the rest of the conventional filters. The THDR and ASA filters are dominated by a large-amplitude response from the shallow prism B1, but the small amplitude responses from the deeper sources A1, C1, D1, E1 and F1 are

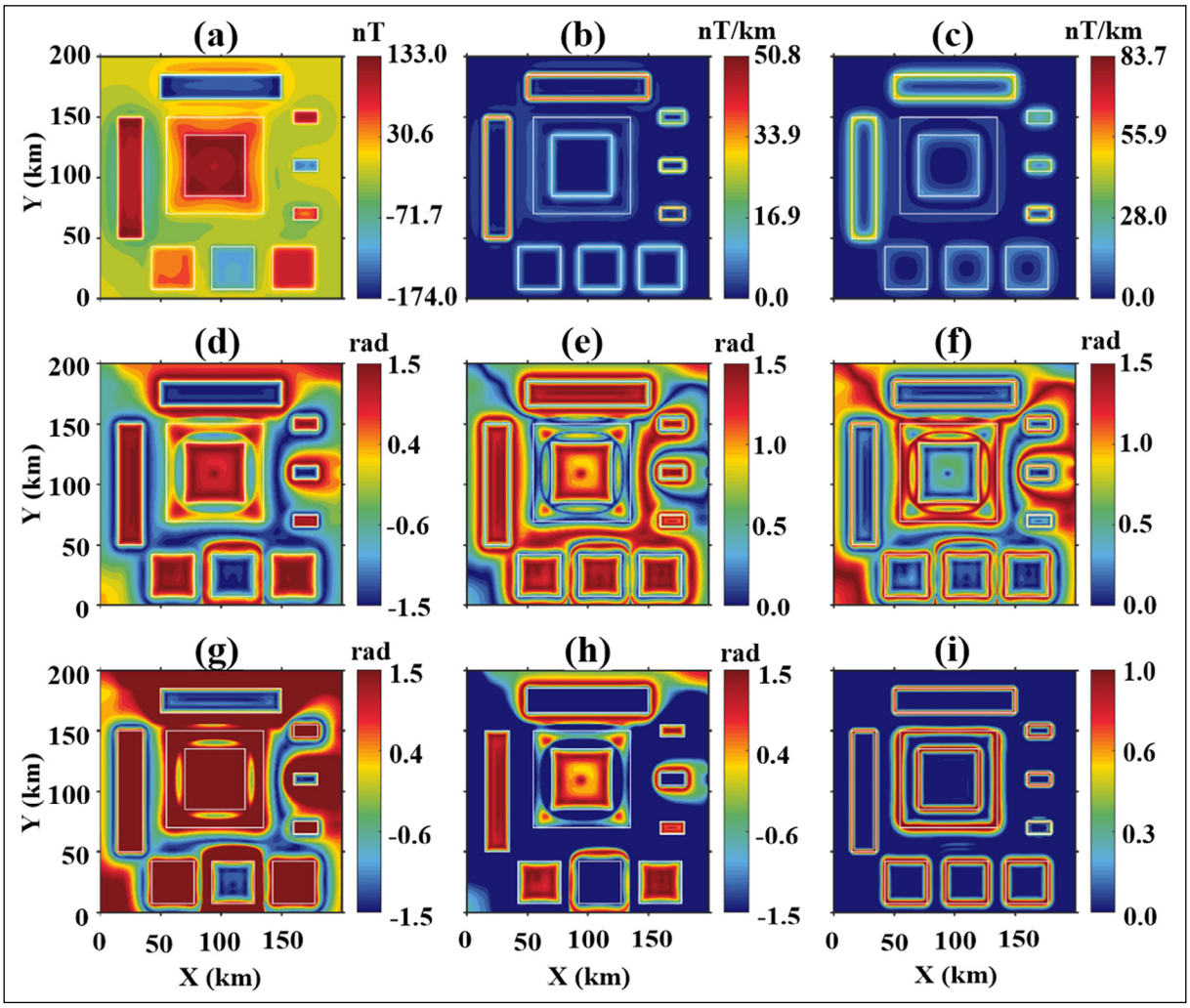

Figure 5- The magnetic anomaly is shown in a); Seven out of 10 bodies are positively magnetized, and the remaining three (2, 4 and 9) are negatively magnetized. The response of various edge detection filters are b) THDR, c) ASA, d) TDR, e) TM, f) TDX, g) TDR + TDX, h) TDR – TDX and i) EG filter (The white line represents the real prism edge).

blurred. Moreover, the maximal amplitude of the ASA filter needs to function better for thin source E1, despite the shallower depth than sources C1, D1 and F1. The TDR (Figure 7d), TM (Figure 7e) and TDX (Figure 7f) filters can balance the edges of the shallow and deep-seated sources well, but they produce such false and spurious edges. The images obtained from using the TDR + TDX (Figure 7g) and TDR-TDX (Figure 7h) filters again show that they do not function well for detecting the sources' edges and produce false contours around and inside of sources. However, their quality and resolution are better than THDR, ASA, TDR, TM and TDX filters. However, the EG filter (Figure 7i) successfully delineates all the edges with minimum influence of the added noise.

6. Application on Aeromagnetic Data

In this section, the ability of the EG filter is tested on the real magnetic data from the northeastern part of the Indiana region situated in North America (Figure 8). The study area consists of gently eastward-dipping sequences of shale, limestone, and sandstone of Paleozoic age formed from material deposited when transgressing shallow seas covered most of the North American continent (Haase et al., 2010). These bedrock units are covered by unconsolidated deposits left from several intervals of glaciation in the Tertiary and Quaternary periods. The bedrock of Indiana experienced erosion at least since late Pennsylvanian time (~300 million years ago). It was

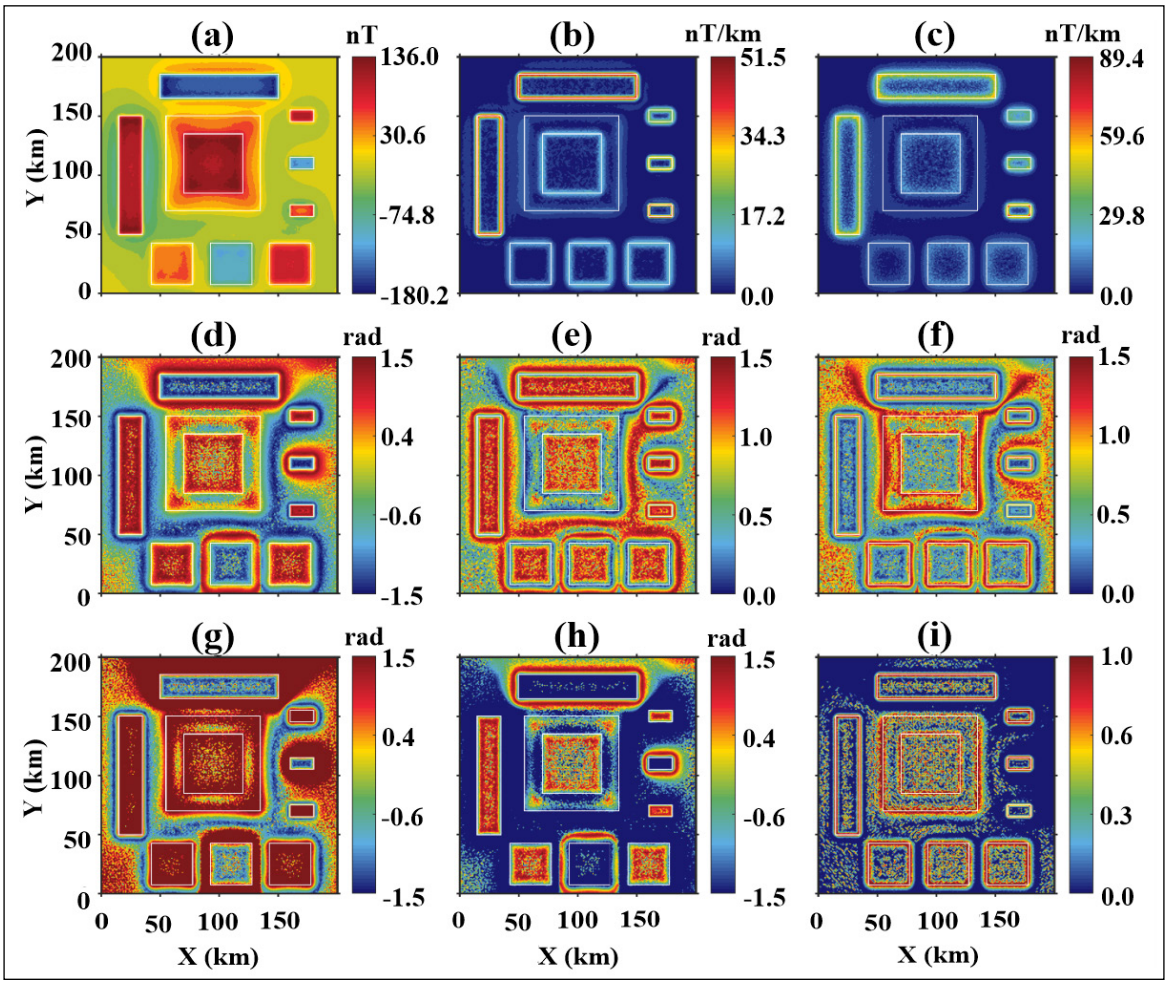

Figure 6- The magnetic anomaly with 4% Gaussian noise added to the synthetic model is shown in a); The response of various edge detection filters are b) THDR, c) ASA, d) TDR, e) TM, f) TDX, g) TDR + TDX, h) TDR – TDX and i) EG filter (The white line represents the real prism edge).

covered by unconsolidated materials only during the past 2 million years when two major glacial advances and retreats crossed the state. Bedrock is exposed only in the south-central part of the state, which was not glaciated, and in localized areas along the Wabash River (Erd and Greenberg, 1960; Huizing and Russell, 1986).

Magnetic anomalies caused by Earth's magnetic field variations make up the upper part of the Earth's crust. The patterns in the magnetic anomalies are used to delineate the locations of buried faults and magnetite-bearing rocks by analyzing the Curie depths and the depth to the base of the sedimentary basin. The analysis of magnetic data is vital for mineral exploration and geological mapping studies. The magnetic anomaly map over the study region, the northeastern part of the Indiana region situated in North America, is constructed from the grids that combine the magnetic data information collected by United States Geological Survey (USGS) during 1947-1994 in 19 separate magnetic surveys due to which the data has varying quality (Henderson and Zietz, 1958; Philbin et al., 1965). These magnetic anomaly maps were digitized along flight-line, considered the most accurate method of recovering the original data. All surveys have been continued to a height of ~300 m above ground and merged to form the States compilation. Index maps show the location of the original surveys, and a data table summarizes the detailed specifications of the surveys. The final magnetic anomaly grid with a 500 m interval and

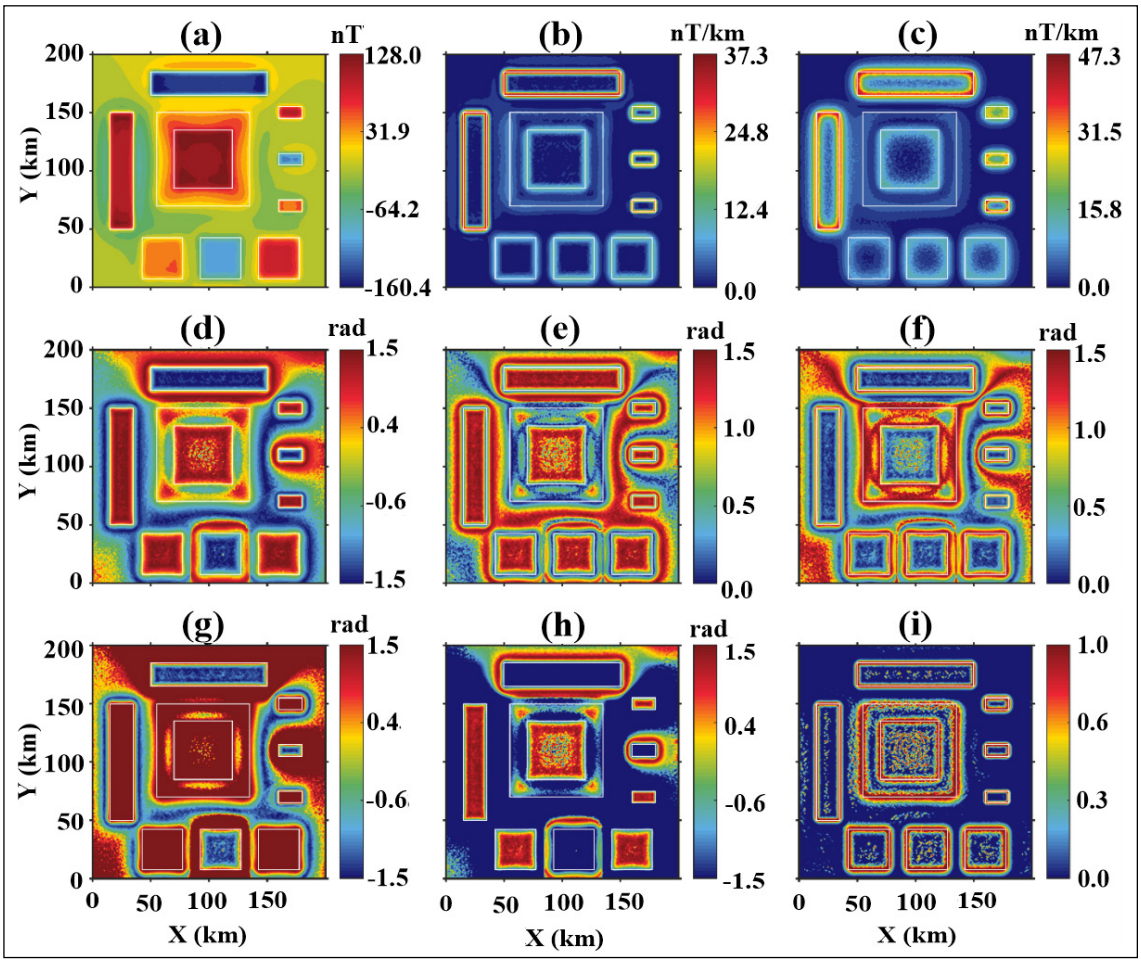

Figure 7- The noise-induced magnetic anomaly continued 500 m upwards is shown in; a) the response of various edge detection filters are b) THDR, c) ASA, d) TDR, e) TM, f) TDX, g) TDR + TDX, h) TDR – TDX and i) EG filter (The white line represents the real prism edge).

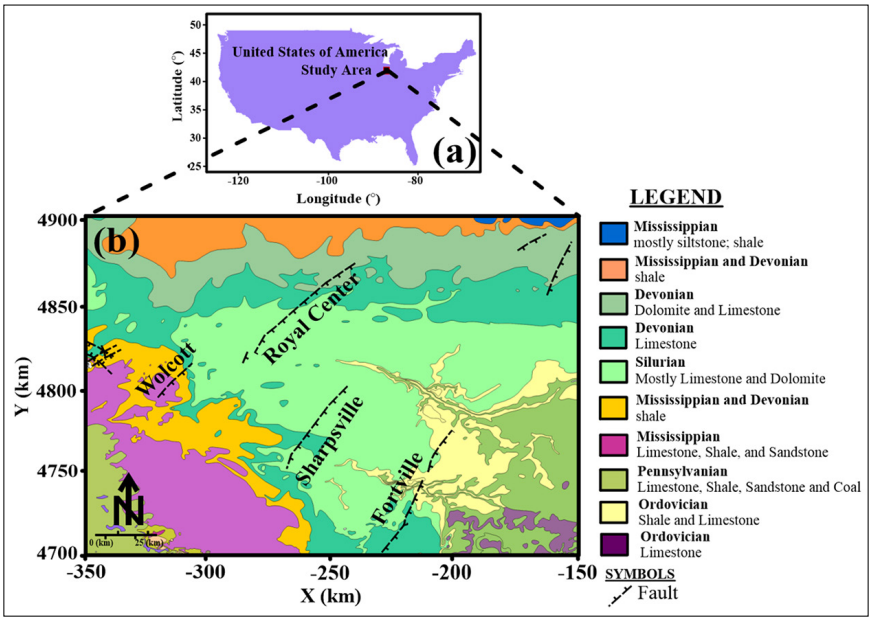

Figure 8- Geological map of the study region with the major tectonic features overlaid (modified from Gray et al., 1987; Gray, 1989 and https://www.usgs.gov).

a part of the magnetic anomaly map is used in the present study and is shown in Figure 9a.

Figures 9b and 9c display the results obtained from using the THDR and ASA filters, respectively. As can be seen, the maps of ASA and THDR are blurred and non-reliable in bringing precise edges for the subsurface sources. Figures 9d, 9e and 9f show the results determined by the TDR, TM and TDX filters, respectively. As seen from these figures, the methods can equalize the amplitudes of large and small anomalies; many adjacent boundaries obtained from this method are connected, making it difficult to detect the geological structures. Figures 9g and 9h show the results of applying TDR+TDX and TDR-TDX, respectively.

The boundaries outlined by the TDR±TDX filters are more precise and accurate than those obtained from other filters. Figure 9i depicts the result obtained by the EG filter on the magnetic data. As observed from the response of the EG filter, it is clear that the detected lineaments have a balanced response from the sources situated at different depths below the subsurface. Moreover, the filter performed better when compared to the other conventional filters used in the present study. Most of the lineaments generated in the study region are trending random direction. The results from the present study are plotted in red, bounded by a sharp blue color line that merely coincides with the existing tectonic features (Figure 10). We can observe that the Fortville fault is directed in almost N-S to N/NE-S/SW has a gravity gradient in the same direction.

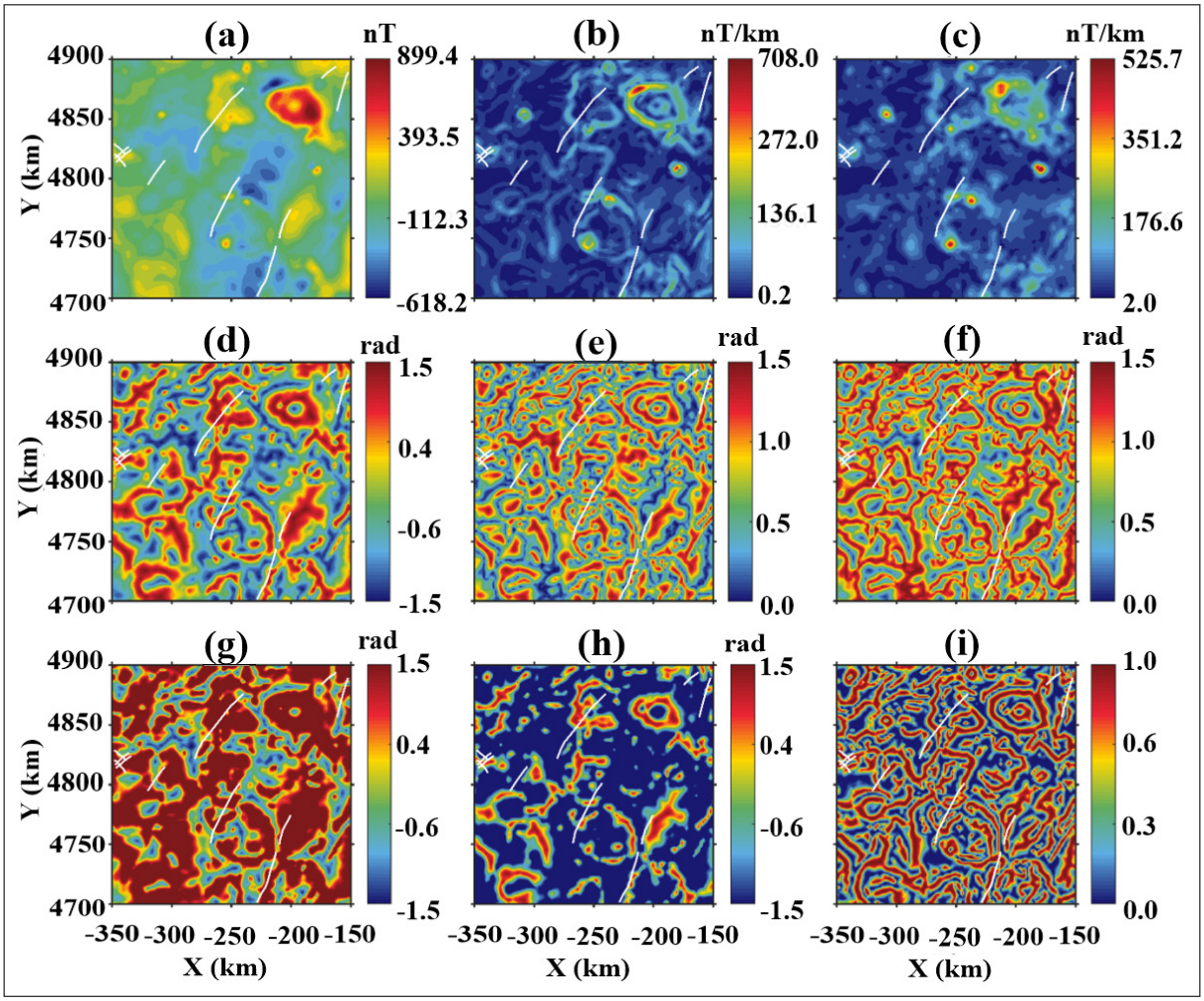

Figure 9- The aero-magnetic anomaly is shown in; a) the response of various edge detection filters are b) THDR, c) ASA, d) TDR, e) TM, f) TDX, g) TDR + TDX, h) TDR – TDX and i) EG filter.

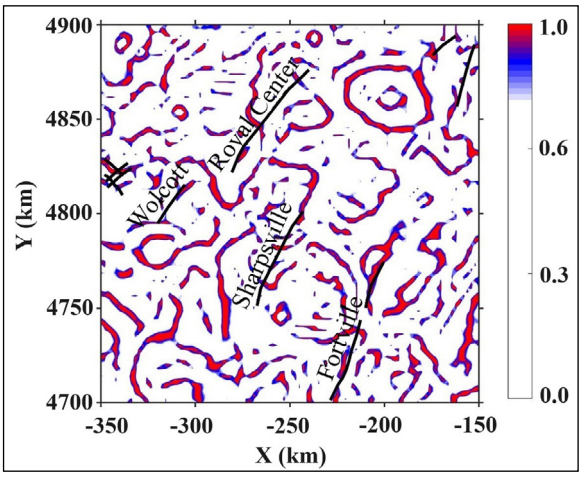

Figure 10-Interpreted lineaments (red color) of the study region overlaid by the major tectonic features (black lines).

However, it has been constrained by a lineament running in the E-W direction towards its northern end. Even though the Sharpsville tectonic fault runs in the N/NE-S/SW direction, we can observe almost crescent-shaped lineaments towards its southern end, followed by an N/NE-S/SW dipping lineament at its northern end. A similar case is seen for the Wolcott tectonic fault. The lineaments beneath the Royal Center tectonic fault are not aligned in the direction of the fault. Instead, the central part of the Royal Center fault is dominated by a N-S trending lineament.

7. Results

Edge detection is a fundamental process in subsurface structural analysis and interpretation. The accuracy increases with noise reduction, making new filters more common. Because the edge enhancement filters are based on the derivative of the anomaly, they amplify the noise signal in the data. However, the EG filter can equalize the weak and strong signals simultaneously and does not bring any false information to the edge map. Also, the EG filter generated a new structural map of the study region in North America, which can help us to draw a new structural and tectonic framework. Finally, the EG is higher resolution, removal of false edges and generates subtler geologic features.

Acknowledgements

The authors would like to thank the US Geological Survey (https://www.usgs.gov) for permission to use the geological information and the aeromagnetic data and Dr. Gordon Robert John Cooper for providing the Hilbert transform calculation scripts.

References

Alvandi, A., Ardestani, V. E. 2023. Edge detection of potential field anomalies using the Gompertz function as a high-resolution edge enhancement filter. Bulletin of Geophysics and Oceanography 64(3), 279-300.

Alvandi, A., Toktay, H. D., Pham, L. T. 2022. Capability of improved logistics filter in determining lateral boundaries and edges of gravity and magnetic anomalies Tuzgölü Area, Türkiye, Journal of Mining Engineering 17(56), 57-72.

Alvandi, A., Toktay, H D., Ardestani, V. E. 2023. Edge detection of geological structures based on a logistic function: A case study for gravity data of the Western Carpathians. International Journal of Mining and Geo-Engineering 57(3), 267-274.

Blakely, R. J., Simpson, R. W. 1986. Approximating edges of source bodies from magnetic or gravity anomalies. Geophysics 51(7), 1494-1498.

Castro, F. R., Oliveira, S. P., De Souza, J., Ferreira, F. J. F. 2018. GRAV-MAG SUITE: An open source MATLAB-based program for processing potential field data. Sociedade Brasileira de Geofísica 8(2), 1-6.

Cooper, G. R. 2009. Balancing images of potential-field data. Geophysics 74(3), 17-20.

Cooper, G. R. J., Cowan, D.R. 2006. Enhancing potential field data using filters based on the local phase. Computers and Geosciences 32(10), 1585-1591.

Cordell, L., Grauch, V. J. S. 1985. Mapping basement magnetization zones from aeromagnetic data in the San Juan Basin, New Mexico. In: The utility of regional gravity and magnetic anomaly maps. Society of Exploration Geophysicists Press, 181-197.

Erd, R. C., Greenberg, S.S. 1960. Minerals of Indiana. Indiana Geological Survey Bulletin 18, 73.

Gray, H. H. 1989. Quaternary geologic map of Indiana: Indiana Geological Survey Miscellaneous Map No: 49, scale 1:500.000, Bloomington, Indiana, United States of America.

Gray, H. H., Ault, C. H., Keller, S. J. 1987. Bedrock geologic map of Indiana, Indiana Geological Survey Miscellaneous Map No: 48, scale 1:500.000, Indiana, United States of America.

Haase, S. H., Park, C. H., Nowack, R. L., Hill, J. R. 2010. Probabilistic seismic hazard estimates incorporating site effects-an example from Indiana, USA. Environmental and Engineering Geoscience 16 (4), 369-388.

Henderson, J. R., Zietz, I. 1958. Interpretation of an aeromagnetic survey of Indiana: US Geological Survey Professional Paper 316-B, 17, scale 1:500,000, Indiana, United States of America

Huizing, T. E., Russell, R. E. 1986. Indiana minerals: a locality index. Rocks and Minerals 61(3),136-151.

Ibraheem, I. M., Tezkan, B., Ghazala, H., Othman, A. A. 2023. A new edge enhancement filter for the interpretation of magnetic field data. Pure and Applied Geophysics 180, 2223-2240.

Miller, H. G., Singh, V. 1994. Potential field tilt—a new concept for location of potential field sources. Journal of Applied Geophysics 32(2-3), 213-217.

Nabighian M. N. 1984. Towards a three-dimensional automatic interpretation of potential field data via generalized Hilbert transforms-fundamental relations. Geophysics 49, 780-786.

Pham, L. T., Oksum, E., Do, T. D., Huy, M. L. 2018. New method for edges detection of magnetic sources using logistic function. Geofizicheskiy Zhurnal 40(6), 127-135.

Pham, L. T., Oksum, E., Do, T. D., Nguyen, D. V., Eldosouky, A.M. 2021. On the performance of phase-based filters for enhancing lateral boundaries of magnetic and gravity sources: a case study of the Seattle uplift. Arabian Journal of Geosciences 14(2), 1-11.

Pham, L. T., Eldosouky, A. M., Oksum, E., Saada, S. A. 2022. A new high-resolution filter for source edge detection of potential field data. Geocarto International 37(11), 3051-3068.

Philbin, P. W., Long, C. L., Moore, F. C. 1965. Aeromagnetic map of the Columbus-Dayton area, Ohio and Indiana: U.S. Geological Survey Geophysical Investigations Map GP-491, scale 1:250,000, United States of America.

Phillips, J. D. 2002. Processing and interpretation of aeromagnetic data for the Santa Cruz Basin-Patagonia mountains area, South-central Arizona. US Geological Survey Open -File Report 02-98, Washington, DC, United States of America.

Prasad, K. N. D., Pham, L. T., Singh, A. P. 2022*a*. A novel filter "ImpTAHG" for edge detection and a case study from Cambay Rift Basin, India. Pure and Applied Geophysics 179(6), 2351-2364.

Prasad, K. N. D., Pham, L. T., Singh, A. P. 2022*b*. Structural mapping of potential field sources using BHG filter. Geocarto International 37, 1-28.

Richards, F. J. 1959. A flexible growth function for empirical use. Journal of Experimental Botany 10(2), 290-301.

Roest, W. R., Verhoef, J., Pilkington, M. 1992. Magnetic interpretation using the 3-D analytic signal. Geophysics 57(1), 116-125.

USGS Science for Changing World (United States Geological Survey). https://www.usgs.gov. 05 August 2024

Wijns, C., Perez, C., Kowalczyk, P. 2005. Theta map: Eedge detection in magnetic data. Geophysics 70(4), L39-L43.

Zuo, B., Hu, X., Liu, S., Geng, M. 2018. Delineation of overlapping magnetic field source boundaries with a 3-D multi-layer convolution model. Journal of Applied Geophysics, 150, 74-83.